Intraoperative Molecular Fluorescence Imaging of Pancreatic Cancer by Targeting Vascular Endothelial Growth Factor: A Multicenter Feasibility Dose-Escalation Study

Babs G. Sibinga Mulder*[1], Marjory Koller*[2], Evelien W. Duiker[3], Arantza Farina Sarasqueta[4], Jakobus Burggraaf[5], Vincent E. de Meijer[2], Alexander L. Vahrmeijer[1], Frederik J.H. Hoogwater[2], Bert A. Bonsing[1], Gooitzen M. van Dam[2,6], J. Sven D. Mieog[1], and Bobby K. Pranger[2]

[1]*Department of Surgery, Leiden University Medical Center, Leiden, The Netherlands;* [2]*Department of Surgery, University of Groningen and University Medical Center Groningen, Groningen, The Netherlands;* [3]*Department of Pathology and Medical Biology, University Medical Center Groningen, Groningen, The Netherlands;* [4]*Department of Pathology, Leiden University Medical Center, Leiden, The Netherlands;* [5]*Center for Human Drug Research, Leiden, The Netherlands and* [6]*AxelaRx/TRACER Europe BV, Groningen, The Netherlands*

Tumor visualization with near-infrared fluorescence (NIRF) imaging might aid exploration and resection of pancreatic cancer by visualizing the tumor in real time. Conjugation of the near-infrared fluorophore IRDye800CW to the monoclonal antibody bevacizumab enables targeting of vascular endothelial growth factor A. The aim of this study was to determine whether intraoperative tumor-specific imaging of pancreatic cancer with the fluorescent tracer bevacizumab-800CW is feasible and safe. **Methods:** In this multicenter dose-escalation phase I trial, patients in whom pancreatic ductal adenocarcinoma (PDAC) was suspected were administered bevacizumab-800CW (4.5, 10, or 25 mg) 3 d before surgery. Safety monitoring encompassed allergic or anaphylactic reactions and serious adverse events attributed to bevacizumab-800CW. Intraoperative NIRF imaging was performed immediately after laparotomy, just before and after resection of the specimen. Postoperatively, fluorescence signals on the axial slices and formalin-fixed paraffin-embedded tissue blocks from the resected specimens were correlated with histology. Subsequently, tumor-to-background ratios (TBR) were calculated. **Results:** Ten patients with clinically suspected PDAC were enrolled in the study. Four of the resected specimens were confirmed PDACs; other malignancies were distal cholangiocarcinoma, ampullary carcinoma, and neuroendocrine tumors. No serious adverse events were related to bevacizumab-800CW. In vivo tumor visualization with NIRF imaging differed per tumor type and was nonconclusive. Ex vivo TBRs were 1.3, 1.5, and 2.5 for the 4.5-, 10-, and 25-mg groups, respectively. **Conclusion:** NIRF-guided surgery in patients with suspected PDAC using bevacizumab-IRDye800CW is feasible and safe. However, suboptimal TBRs were obtained because no clear distinction between pancreatic cancer from normal or inflamed pancreatic tissue was achieved. Therefore, a more tumor-specific tracer than bevacizumab-IRDye800CW for PDAC is preferred.

Key Words: near-infrared fluorescence imaging; molecular fluorescence imaging; pancreatic cancer

J Nucl Med 2023; 64:82–89
DOI: 10.2967/jnumed.121.263773

Currently, the only curative treatment for pancreatic cancer is radical surgery (R0 resection). However, a radical resection is achieved in only a minority of the patients. Surgery with curative intent may be aborted during the procedure when exploratory laparotomy reveals locally advanced disease (e.g., arterial encasement) or distant metastases (*1*,*2*). Because of the quick spread of pancreatic cancer cells via perineural and perivascular pathways, occult metastases and tumor growth in resection margins can easily be missed (*3*). Besides intraoperative frozen section analysis and ultrasonography, surgeons typically rely on visual inspection and palpation alone to distinguish between tumorous and benign tissue and to detect remaining small tumor deposits or locoregional metastases. Because of these limitations, positive resection margin rates are reported to be as high as 50%–75% (*4*).

Improved visualization of resection margins and detection of small tumor deposits is highly desirable in pancreatic cancer surgery to prevent under- or overtreatment. A relatively new technique that can fulfill this unmet need is intraoperative near-infrared fluorescence (NIRF) imaging (*5*). The main advantages of NIRF imaging are the real-time and ideally tumor-specific visual feedback to the surgeon, thereby enabling differentiation between benign and malignant tissue during surgery and enhancing visualization of small tumor deposits (*6*). A tumor-specific fluorescent tracer will accumulate in or bind to the tumor after intravenous administration. Subsequently, fluorescence signals can be detected using dedicated imaging systems. Recent studies showed promising results using tumor-specific NIRF imaging for the visualization of several cancer types (*7*–*10*). However, successful and tumor-specific visualization of pancreatic cancer using NIRF imaging remains challenging because of several factors, such as the frequent presence of the desmoplastic stroma reaction or periinflammatory tissue reaction.

Vascular endothelial growth factor (VEGF) is involved in tumor-induced angiogenesis and lymph angiogenesis in most solid tumors (*11*). Several studies report an overexpression of VEGF in pancreatic cancer tissue compared with normal pancreatic tissue (*12*,*13*). Bevacizumab is an antibody directed toward VEGF-A–overexpressing tumors, and by coupling the antibody to the organic fluorophore IRDye800CW, a tumor-specific NIRF tracer (bevacizumab-800CW) was developed. Bevacizumab-800CW has already been shown to be a valid and safe tracer for molecular imaging in several solid cancer types (*8*,*9*,*14*,*15*).

Received Jan. 17, 2022; revision accepted Jun. 2, 2022.
For correspondence or reprints, contact Bobby K. Pranger (b.k.pranger@umcg.nl).
*Contributed equally to this work.
Published online Jun. 9, 2022.

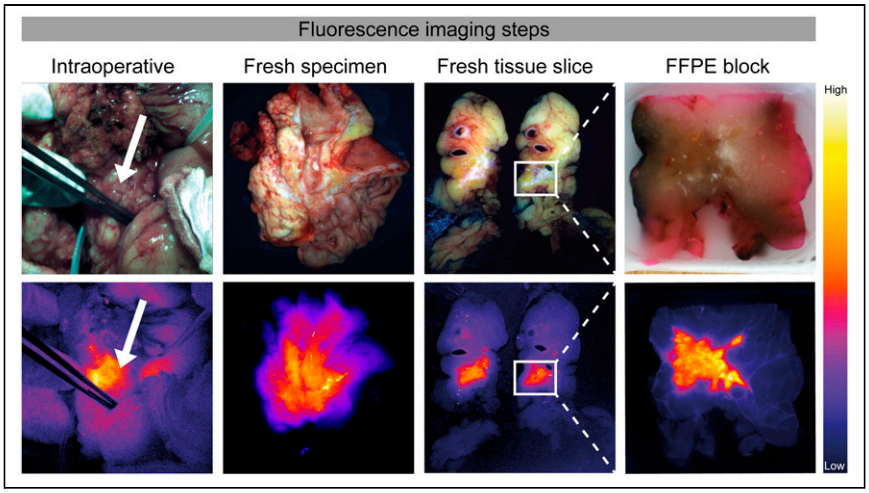

FIGURE 1. Workflow from intraoperative to FFPE blocks enabling correlation of intraoperative fluorescence signals with histopathology. Intraoperative color images and corresponding fluorescence images are obtained in vivo during surgery. Then, imaging of fresh surgical specimen followed by serial slicing is performed. Imaging of fresh tissue slices is followed by paraffin embedding. Imaging of FFPE blocks is done to determine TBR. Arrows show tumor area.

The aim of this study was to determine whether intraoperative tumor-specific imaging of pancreatic cancer is feasible and safe using the fluorescent tracer bevacizumab-800CW.

MATERIALS AND METHODS

Patient Population

This study was approved by the certified medical ethics review board of the University Medical Center Groningen and Leiden University Medical Center (clinicaltrials.gov identifier NCT02743975). The study was performed in accordance with the ethical principles of Helsinki (adapted version; Fortaleza, Brazil, 2013) and the laws and regulations of The Netherlands. All patients provided written informed consent before participation in the study. A safety monitoring board was appointed before the start of the clinical trial. All serious adverse events during or after surgery were reported immediately to the investigational review board of the University Medical Center Groningen, the data safety monitoring board, and the Dutch Central Committee on Research Involving Human Subjects.

Patients older than 18 y with a clinical suspicion of pancreatic ductal adenocarcinoma (PDAC) and scheduled to undergo surgery with curative intent were included in this single-arm, open-label multicenter study. All patients had a World Health Organization performance score of 0–2. Patients who underwent neoadjuvant treatment or had a concurrent invasive malignancy were excluded. Other exclusion criteria were medical or psychiatric conditions compromising the patient's ability to give informed consent, pregnancy or lactation, a history of infusion reactions to bevacizumab, inadequately controlled hypertension or a history of myocardial infarction, transient ischemic attack, cerebrovascular accidents, pulmonary embolism, uncontrolled chronic hepatic failure, or unstable angina pectoris 6 mo before inclusion.

Study Design

The primary objective was to identify the optimal dose for visualization of tumor tissue. The secondary objective was to determine whether bevacizumab-800CW could safely be used to identify PDAC with NIRF imaging.

Therefore, a 2-part 4 × 3 dose-finding study design was used. Part I consisted of 4 intravenously administered ascending doses of 4.5 mg, 10 mg, 25 mg, and 50 mg of bevacizumab-800CW 3 d before the planned surgery to 3 patients each. In part II, the defined optimal dose group would be increased to 10 patients to obtain sufficient data points. The optimal dose group would be chosen on the basis of ex vivo tumor-to-background ratio (TBR). Interim analyses were performed after completion of each cohort for the evaluation of intraoperative fluorescence signals, analyses of the ex vivo TBRs, and safety outcomes.

Bevacizumab-IRDye800CW

Bevacizumab-IRDye800CW was produced in the good-manufacturing-practice–certified facility of the University Medical Center Groningen Hospital Pharmacy by conjugating bevacizumab (Roche AG) and IRDye-800CW-NHS (LI-COR Biosciences Inc.) under regulated conditions (*16*).

TABLE 1
Patient and Tumor Characteristics

	Patient				Tumor		
Dose	*n*	Age (y)	Sex	WHO score	Histology	TNM stage	Radicality
4.5 mg	1	64	F	0	Distal cholangiocarcinoma	pT3N1	R0
	2	67	M	1	PDAC	pT3N1	R0
	3	75	M	0	PDAC	pT3N0	R0
	4	69	M	1	Autoimmune pancreatitis	—	—
10 mg	5	56	M	1	Ampullary carcinoma	pT3N1	R0
	6	73	F	0	PDAC	pT3N1	R1
	7	74	F	0	Intrapapillary mucinous neoplasm	—	R0
25 mg	8	47	F	0	PDAC	pT3N2	R0
	9	74	F	0	Ampullary carcinoma	pT3N1	R1
	10	67	M	0	Neuroendocrine tumor	pT3N0	R0

WHO = World Health Organization; R0 = radical resection; R1 = not radical.

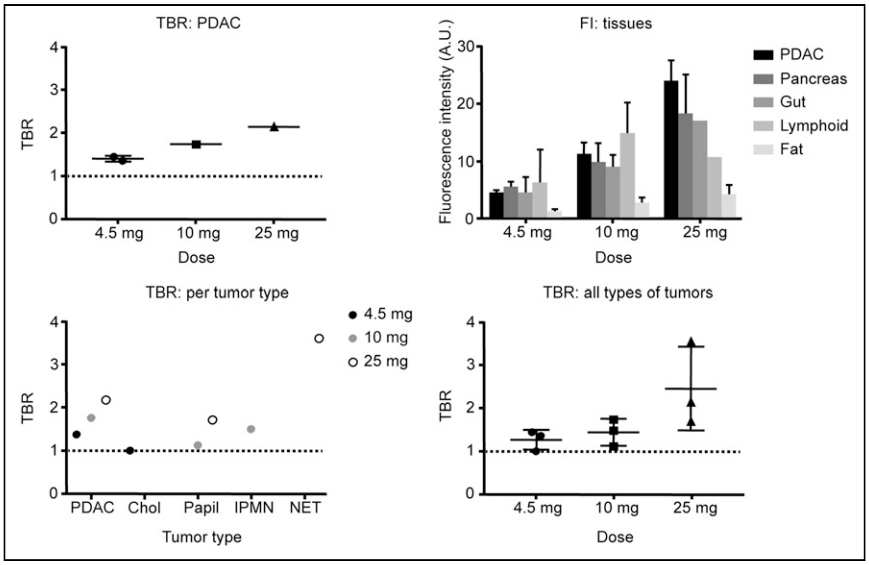

FIGURE 2. TBR and fluorescence intensity (FI). In first row, TBRs of all PDACs distributed per dose group and fluorescence intensity of different tissue types in patients with PDAC are shown. In second row, mean TBR per tumor type distributed per dose group and mean TBRs of all types of tumors distributed per dose group are shown. Chol = distal cholangiocarcinoma; IPMN = intraductal papillary mucinous neoplasm; NET = neuroendocrine tumor; Papil = ampullary carcinoma.

IRDye800CW has excitation and emission maxima at 774 and 789 nm, respectively.

Imaging Systems

Intraoperative imaging was done with a fluorescence camera dedicated to the detection of IRDye-800CW-NHS (SurgVision BV). The system was configured with 2 light-emitting diode lights for 800 nm of illumination and 1 light-emitting diode light for white-light illumination. Real-time color and NIRF images were simultaneously collected. The imaging device was approved for intraoperative application in humans by the technical departments of the University Medical Center Groningen and Leiden University Medical Center. Ex vivo imaging was performed using the Blackbox (SurgVision BV) or the Pearl Imager (LI-COR Biosciences Inc.). For detection of fluorescence in formalin-fixed paraffin-embedded (FFPE) blocks, the Odyssey CLX fluorescence flatbed scanning system (LI-COR Biosciences Inc.) was used.

Procedures

Figure 1 shows the NIRF imaging workflow as based on a proposed standardization protocol (*9*). Before surgery, all patients underwent staging laparoscopy to exclude the possibility that the disease was locally advanced or metastatic. Patients received bevacizumab-800CW 3 d before surgery as an intravenous bolus injection. Tolerability assessments (electrocardiography, blood pressure, pulse, peripheral oxygen saturation, respiratory rate, and temperature) were performed just before tracer injection, shortly after tracer injection, and 1 h after tracer injection.

Surgery was performed according to standard practice. Surgeons were not allowed to excise additional tissue exclusively on the basis of fluorescence signals detected intraoperatively. NIRF imaging was performed at 3 predefined time points: the first was after laparotomy, during which all surrounding organs were imaged and fluorescence intensity was determined (if nonspecific background fluorescence signals were present, these were noted); the second was after full preparation of the specimen just before resection (the fluorescence intensity of the expected tumor and the normal pancreatic tissue was noted); and the third was after resection of the specimen, during which the remaining tissue was imaged. If the near-infrared camera detected additional lesions that were not part of the intended resection, the surgeon was allowed to perform a biopsy for postoperative pathologic analysis.

After resection, the gross specimen was imaged. After formalin fixation, the specimen was sliced in 0.3- to 0.5-cm-thick slices according to the preferred protocol (*4*,*17*). All slices were macroscopically examined and imaged. Those slices considered relevant for the pathologist were processed for histologic assessment. The selection of tissue for embedding in FFPE blocks was not altered by fluorescence signal. However, after the pathologist selected slices for diagnostic purposes, an additional slice with high fluorescence signal that was not initially selected by the pathologist as relevant could be embedded apart from the standard of care. We did VEGF staining on 4-μm tissue slides of FFPE tissue blocks containing both tumor and background tissue in all patients (described in the supplemental materials, available at http://jnm.snmjournals.org). After microscopic evaluation and the final pathology report, regions of interest were correlated on the corresponding histologic slice, the FFPE blocks were imaged, and the TBRs were determined on the fluorescence images of the FFPE blocks. Additional information about the tracer, imaging procedures, and pathologic processing is provided in the supplemental materials.

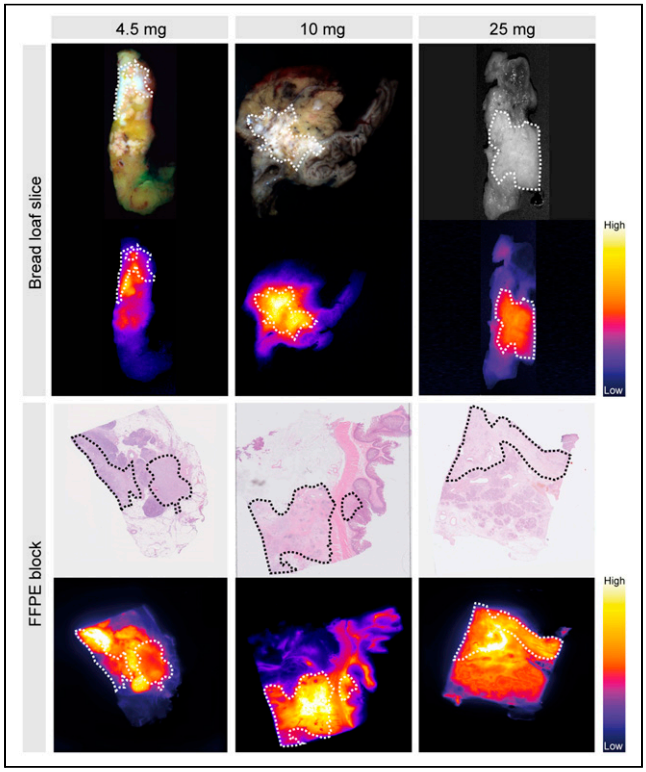

FIGURE 3. Representative images per dose group of PDAC. In first row are white-light image and, below, corresponding representative fluorescence image. Third row contains hematoxylin and eosin sections and, below, corresponding representative fluorescence image. Tumor tissue is delineated with dashed lines.

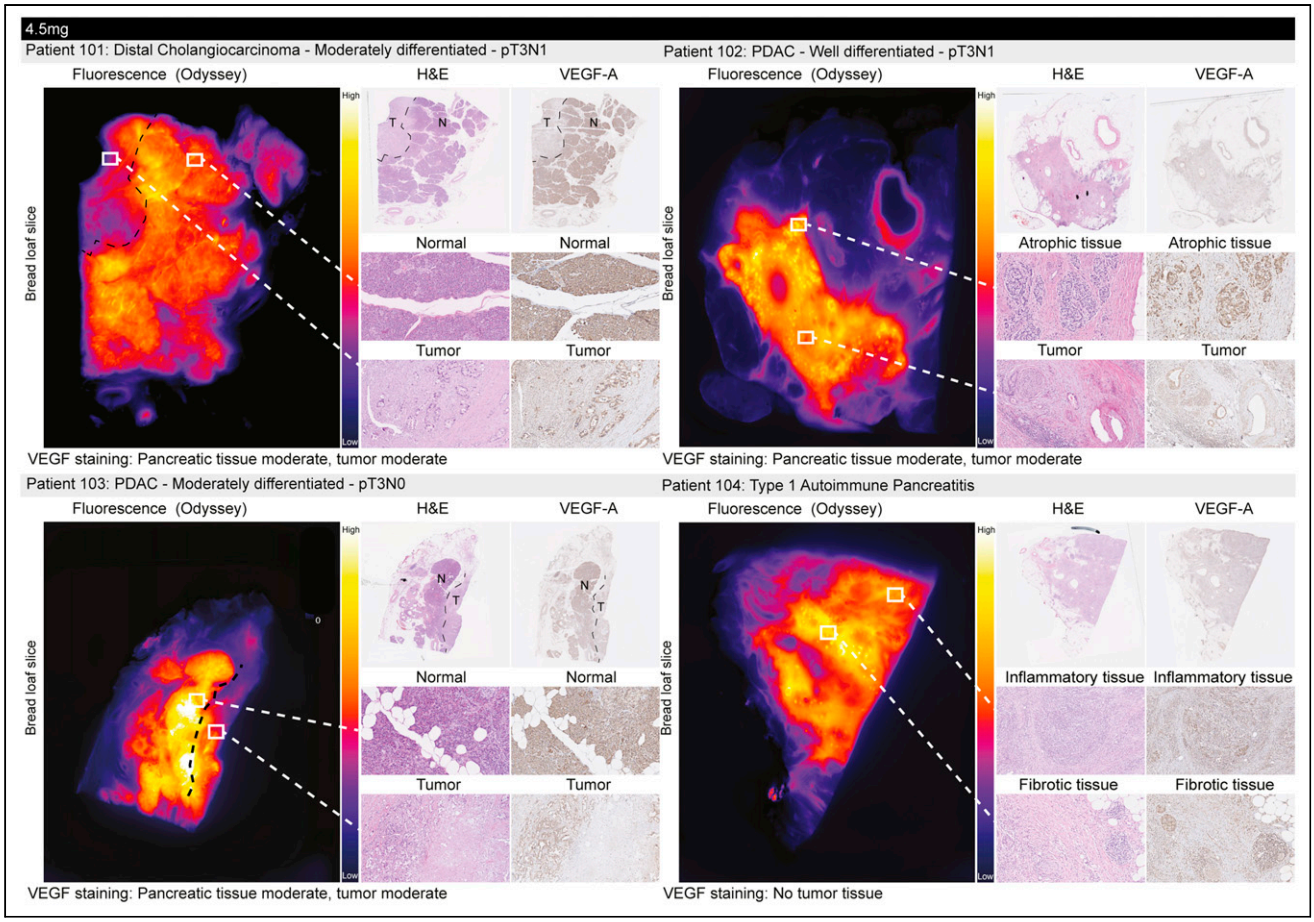

FIGURE 4. In 4.5-mg cohort, representative fluorescence images of bread loaf slice, hematoxylin and eosin staining of bread loaf slice, and VEGF-A staining of bread loaf slice, along with close-ups of hematoxylin and eosin staining and VEGF-A staining. Tumor tissue is delineated, when possible, with black dashed line. H&E = hematoxylin and eosin; N = normal pancreatic tissue; T = tumor.

Fluorescence Quantification

Ex vivo TBRs were calculated on fresh serially sliced tissues (so-called bread-loaf slices). The tumor and the surrounding nontumor tissue were precisely delineated on standard hematoxylin and eosin histopathologic slides by a pathologist masked to fluorescence. An overlay with fluorescent tissue slices was based on anatomic landmarks. Afterward, the ex vivo TBR was calculated as the mean fluorescence intensity (MFI, arbitrary unit) of pancreatic cancer tissue divided by the MFI of the background. The background MFI was calculated on all nontumor tissue for every tissue slice.

Statistics

Descriptive statistics were reported as mean with SD, whereas median with range was used when there was a skewed distribution. Fluorescence signals in tumor and normal tissue were compared using the Mann–Whitney test. A P value of less than 0.05 was considered statistically significant. For descriptive statistics, SPSS (version 23.0) was used; graphs were designed with GraphPad Prism (version 7.0).

RESULTS

Patient and Safety Data

Between December 1, 2016, and February 26, 2018, 10 patients were enrolled with suspected pancreatic ductal carcinoma. Table 1 provides an overview of patient characteristics and tumor characteristics per patient (patients 1–10). After completion of the 4.5-, 10-, and 25-mg dose groups in part I of the study, the investigational review board mandated termination of the study because of low TBRs. In 9 patients, the tracer was administered 3 d before surgery. In patient 3, imaging was performed 10 d after administration of 4.5 mg of tracer because of a postponed exploration due to an adverse event the day before surgery. Therefore, 1 additional patient was included in the first dose group (4.5 mg). No allergic or anaphylactic reactions related to bevacizumab-IRDye800CW were noted. Two serious adverse events were reported, both of which developed in patient 5 and were attributed to the pancreatoduodenectomy. These included a pancreatic fistula requiring percutaneous drainage and antibiotic treatment and, 27 d after surgery, bleeding of the gastroduodenal artery stump requiring radiologic coiling. All safety data are provided in Supplemental Table 1. On the basis of the final histology of the resected specimens, various malignancies were found in the study: PDAC (n = 4), distal cholangiocarcinoma (n = 1), carcinoma of the ampullary region (n = 2), well-differentiated grade 3 neuroendocrine tumor of the pancreas (n = 1), and a low-grade intraductal papillary mucinous neoplasm (n = 1). In patient 4, an autoimmune pancreatitis instead of malignancy was diagnosed on histology.

In Vivo and Ex Vivo Imaging per Tumor Type

PDAC. The approximate location of the expected primary tumor could be visualized with NIRF imaging in vivo with all tested doses of the tracer. However, the primary tumor was difficult to distinguish from normal or fibrotic pancreatic tissue. After resection of the pancreatic head (in patient 6), the pancreatic tail remnant was clinically

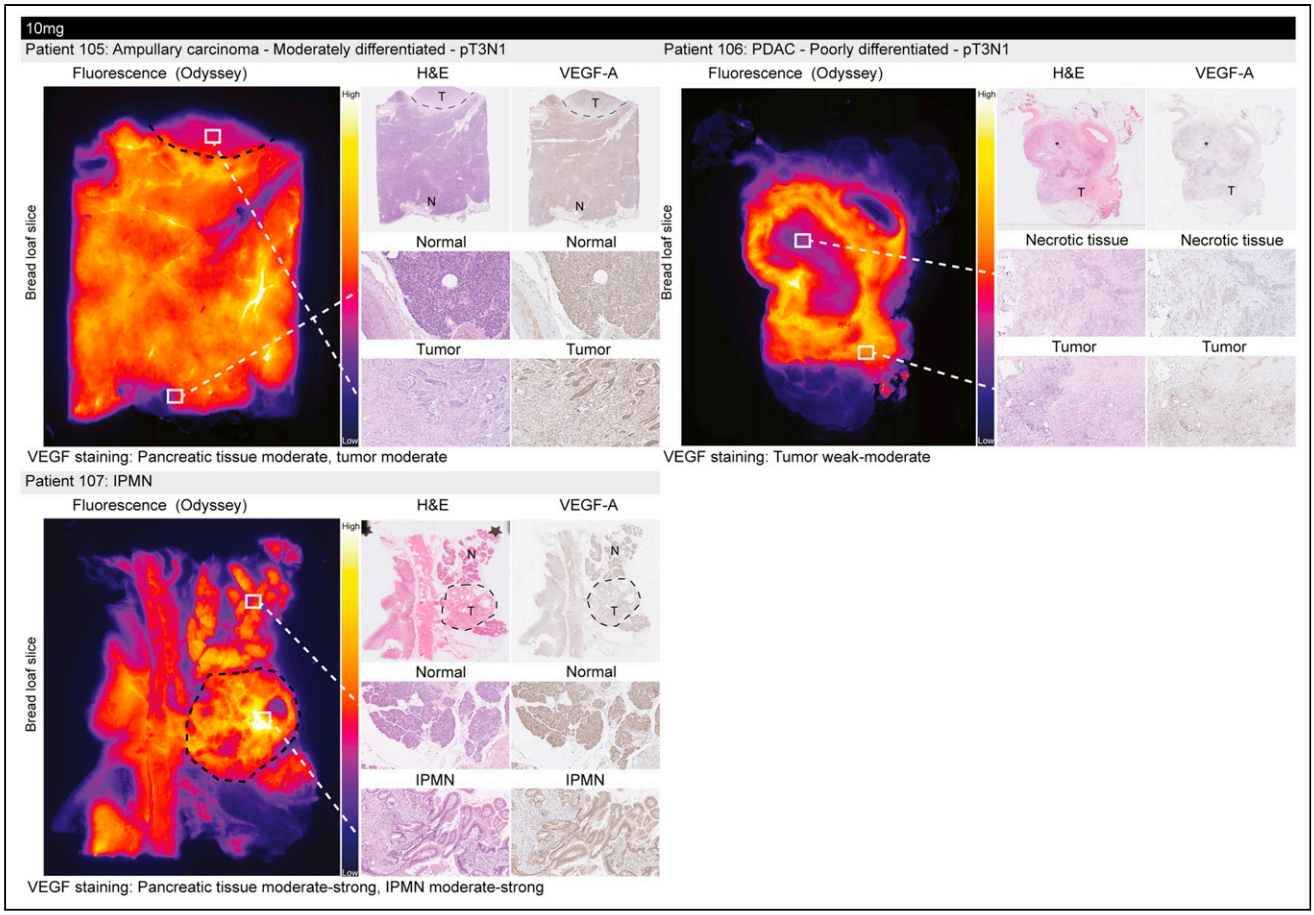

FIGURE 5. In 10-mg cohort, representative fluorescence images of bread loaf slice, hematoxylin and eosin staining of bread loaf slice, and VEGF-A staining of bread loaf slice, along with close-ups of hematoxylin and eosin staining and VEGF-A staining. Tumor tissue is delineated, when possible, with black dashed line. H&E = hematoxylin and eosin; IPMN = intraductal papillary mucinous neoplasm; N = normal pancreatic tissue; T = tumor.

suspected of harboring residual tumor and also showed high fluorescence. The suspicion of malignancy was confirmed by intraoperative ultrasound, and the pancreatic tail was therefore resected. Histologic assessment showed a poorly differentiated tumor in the head, body, and tail of the pancreas, with the tail involvement not being diagnosed during the preoperative work-up. In the other PDAC patients, nonspecific fluorescence signals remained visible after resection of the pancreatic head. Histologic assessment confirmed radical resection. The MFI increased with each dose group, resulting in TBRs of 1.4 (n = 2), 1.7 (n = 1), and 2.1 (n = 1) in the 4.5-, 10-, and 25-mg dose groups, respectively (Fig. 2). Figure 2 demonstrates the contrast between tumorous and other types of tissue based on difference in fluorescence intensity. Representative fluorescence images of specimen slices and FFPE blocks of PDAC per dose group are shown in Figure 3. VEGF staining of the tissue slides showed moderate VEGF expression of normal pancreatic tissue and moderate to strong VEGF expression in tumor tissue of well-differentiated or moderately differentiated cancers. In poorly differentiated tumor tissue, the VEGF expression was weak (Figs. 4–6).

Distal Cholangiocarcinoma. We could not visualize fluorescence signals at the site where the tumor was expected in vivo (patient 1, 4.5 mg). On the specimen slices and FFPE blocks, the MFI was similar between tumor and normal tissue, resulting in a TBR of 1.0 (Fig. 2). VEGF staining of the tissue slides showed moderate VEGF expression of both tumor tissue and normal pancreatic tissue (Fig. 4).

Carcinoma of Ampullary Region. The location of the expected primary tumor could be visualized with NIRF imaging in 2 patients administered either 10 or 25 mg of the tracer in vivo. In patient 8, tumor invasion in the superior mesenteric vein was clinically suspected, and therefore, a wedge resection of the superior mesenteric vein was performed. NIRF imaging of the wedge was positive for tumor. Histologic assessment of the wedge confirmed ingrowth of malignant cells in the vascular wall. On the specimen slices and FFPE blocks, the MFI was similar between tumor and normal tissue, resulting in a TBR of 1.1 and 1.7 for 10 and 25 mg, respectively (Fig. 2). VEGF staining of the tissue slides showed moderate VEGF expression of normal pancreatic tissue and moderate to weak VEGF expression of tumor tissue (Figs. 5 and 6).

Neuroendocrine Neoplasm. The expected location of the tumor was clearly visible with NIRF imaging in vivo; after resection, fluorescence signals diminished strongly. On the specimen slices and FFPE blocks, the MFI significantly differed between tumor and normal tissue (27.6 vs. 7.8, P = 0.04), resulting in a TBR of 3.6 (Fig. 2). VEGF staining of the tissue slides showed weak VEGF expression of tumor tissue and moderate VEGF expression of normal pancreatic tissue (Fig. 6).

Intraductal Papillary Mucinous Neoplasm. The location of the expected primary tumor could be visualized with NIRF imaging in vivo (patient 7; 10 mg), although a clear distinction between pancreatic and tumorous tissue could not be made. On the specimen slices and FFPE blocks, the MFI did not significantly differ

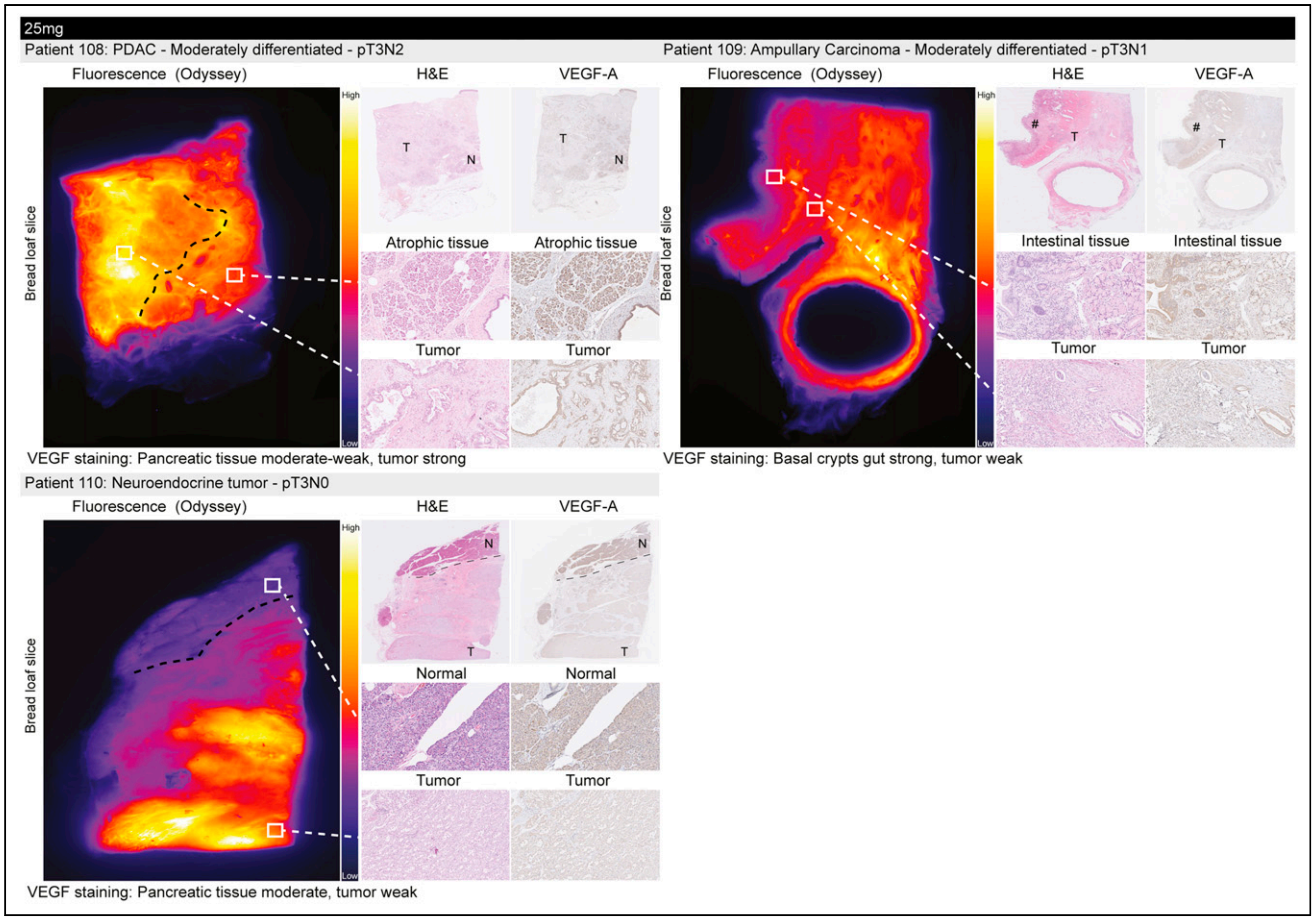

FIGURE 6. In 25-mg cohort, representative fluorescence images of bread loaf slice, hematoxylin and eosin staining of bread loaf slice, and VEGF-A staining of bread loaf slice, along with close-ups of hematoxylin and eosin staining and VEGF-A staining. Tumor tissue is delineated, when possible, with black dashed line. H&E = hematoxylin and eosin; N = normal pancreatic tissue; T = tumor.

between intraductal papillary mucinous neoplasm and normal tissue (84.5 vs. 56.7, $P = 0.40$, resulting in a TBR of 1.5) (Fig. 2). VEGF staining of the tissue slides showed moderate to strong VEGF expression of both intraductal papillary mucinous neoplasm tissue and pancreatic tissue (Fig. 5).

Autoimmune Pancreatitis. In patient 4, the location of the expected tumor could be visualized with fluorescence imaging (4.5 mg). With ex vivo histology, extensive fibrotic and inflammatory tissue was seen and no normal pancreatic tissue was found. Therefore, there was no difference in fluorescence intensity in the resected specimen of the patient with autoimmune pancreatitis (MFI, 50.7). VEGF staining of the tissue slides showed weak VEGF expression in the extensive fibrotic and inflammatory tissue (Fig. 4).

The ex vivo TBRs of all types of tumors together, divided per dose group, are demonstrated in Figure 2. TBRs were 1.3, 1.5, and 2.5 for 4.5, 10, and 25 mg, respectively. Finally, we looked into additional immunohistochemical staining with hypoxia-inducible factor 1-α and added 2 representative slides to Supplemental Figure 1. Hypoxia-inducible factor 1-α staining showed a pattern similar to VEGF-A staining, although expression of hypoxia-inducible factor 1-α was less strong than VEGF-A.

DISCUSSION

In this study, the feasibility and safety of visualizing pancreatic cancer tissue with bevacizumab-800CW were assessed. Intravenous administration of bevacizumab-800CW (i.e., a flat dose of 4.5, 10, and 25 mg) 3 d before surgery appeared safe, as no changes in safety parameters (including vital signs and electrocardiography) occurred, nor did any related adverse events. Both in vivo and ex vivo NIRF imaging of pancreatic cancer tissue was feasible with bevacizumab-800CW, as fluorescence signals could be detected in tumor tissue. However, suboptimal TBRs were obtained, and pancreatic cancer tissue could not reliably be distinguished from normal pancreatic tissue.

NIRF imaging with other tracers in previous clinical trials had similar results. The feasibility of SGM-101, a monoclonal antibody against carcinoembryonic antigen labeled with 700-nm fluorophore, was assessed for intraoperative NIRF imaging of PDAC. SGM-101 could reach and bind carcinoembryonic antigen–expressing tumor cells, but with modest in vivo TBRs (1.6 for primary tumors) (*18*). With cetuximab-IRDye800, detection of pancreatic cancer tissue and tumor-bearing lymph nodes was feasible. Studies with larger patient numbers must show whether this tracer is indeed suitable for in vivo NIRF imaging of pancreatic cancer (*19*).

Limited success rates for treating PDAC with systemically administered agents are commonly attributed to the desmoplastic stroma of PDAC, which is thought to severely reduce the delivery of these therapies by an increased intratumoral pressure gradient and the presence of fibrotic tissue. However, cetuximab, bevacizumab, and the carcinoembryonic antigen–targeting antibody are full-sized monoclonal antibodies and managed to penetrate the dense desmoplastic stroma and bind pancreatic cancer cells and endothelial cells.

The results of these NIRF imaging studies for detection of pancreatic cancer suggest that pancreatic tumor tissue might be difficult to detect intraoperatively using fluorescent tracers. The yield of tumor-specific imaging in the current study was lower than expected, and therefore, the study was terminated early. The most obvious reasons for suboptimal pancreatic cancer visualization with NIRF are the unfavorable intrinsic characteristics of pancreatic cancer. Because of the previously mentioned desmoplastic stroma, poor vascularization, and high intratumoral pressure, the antibody-based tracers might not accumulate optimally in the tumor as compared with the surrounding tissue, making it difficult to distinguish normal tissue from tumor tissue. In this study, the difficulty in demonstrating tumor-specific fluorescence imaging could also be due to a suboptimal choice of the target VEGF-A, a soluble factor present for angiogenesis in the stroma of tumor tissue. An FG-domain messenger RNA profiling study on a set of normal pancreatic tissue and PDAC tissue identified THY1, CTSE, GGT5, and MUC1 as potential targets for pancreatic cancer imaging (*20*). Other targets that are potentially suitable for NIRF imaging of pancreatic tumors are integrin $\alpha v\beta 6$ and urokinase-type plasminogen activator receptor (*21*). Furthermore, future studies should focus on a tracer that can differentiate between chemotherapy-induced fibrotic tissue and vital cancer cells, because an increased number of patients will be treated with neoadjuvant therapy. Preclinical studies showed promising results for fluorescence-guided surgery in combination with neoadjuvant chemotherapy and treatment of minimal residual cancer after fluorescence-guided surgery in pancreatic cancer (*22–24*).

Moreover, the detection of metastases is important in assessing the optimal treatment strategy for pancreatic cancer patients. Identification of preoperatively missed metastases via preoperative staging laparoscopy with NIRF imaging might be of great value for these patients. Resection of the primary tumor does not improve the prognosis in metastasized patients—only delaying appropriate treatment (*25*). In this setting, a tumor-specific tracer should be used that is not metabolized by the liver, because pancreatic cancer preferably metastasizes to the liver. A potential tracer could be cRGD-ZW800-1, which is renally cleared. Preclinical studies showed promising results for pancreatic cancer detection (*26*). cRGD-ZW800-1 is currently being tested in patients with colorectal tumors and, if promising, will be expanded to pancreatic cancer patients (clinicaltrials.gov identifier NL6250805817). Another promising tracer is panitumumab-IRDye800CW. This tracer proved to be safe and feasible to use for fluorescence-guided surgery in patients with pancreatic cancer undergoing surgical intervention and has the potential to improve patient selection and enhance visualization of surgical margins, metastatic lymph nodes, and distant metastasis (*27*).

A unique aspect of our study was the variety of cancer types that were included; besides PDAC, other tumors visualized with bevacizumab-800CW included neuroendocrine tumors, distal cholangiocarcinoma, an intraductal papillary mucinous neoplasm, and ampullary tumors. Tumor-targeted NIRF imaging of these tumors has not yet been described. In neuroendocrine tumors, we observed a 3-fold higher signal intensity from the tumor than from the background. This finding most likely reflects the enhanced permeability and retention effect by which high-molecular-weight nontargeted drugs and prodrugs accumulate in tissues that offer increased vascular permeability.

CONCLUSION

NIRF-guided surgery in patients with suspected pancreatic cancer using bevacizumab-IRDye800CW is feasible and safe. However, suboptimal TBRs were obtained, and consequently, distinguishing pancreatic cancer tissue from normal pancreatic tissue remains challenging.

DISCLOSURE

The research leading to the results was supported by an unrestricted research grant from SurgVision BV. Marjory Koller and Gooitzen van Dam report receiving grant 602812 from the FP-7-Framework Program Betacure during the study. This work was supported by the Bas Mulder Award (grant UL2015-7665) from the Dutch Cancer Society. No other potential conflict of interest relevant to this article was reported.

KEY POINTS

QUESTION: Is NIRF-guided surgery using the tracer bevacizumab-800CW feasible and safe in patients with suspected PDAC?

PERTINENT FINDINGS: In this clinical trial, we showed that NIRF-guided surgery in patients with suspected PDAC using bevacizumab-800CW is feasible and safe. However, suboptimal TBRs were obtained because no clear distinction between pancreatic cancer and normal or inflamed pancreatic tissue was possible.

IMPLICATIONS FOR PATIENT CARE: Although suboptimal TBRs were obtained in pancreatic cancer, we showed that full-sized monoclonal antibodies manage to penetrate the dense desmoplastic stroma and bind to pancreatic cancer cells and endothelial cells.

REFERENCES

1. Campbell F, Smith RA, Whelan P, et al. Classification of R1 resections for pancreatic cancer: the prognostic relevance of tumour involvement within 1 mm of a resection margin. *Histopathology.* 2009;55:277–283.
2. Ghaneh P, Kleeff J, Halloran CM, et al. The impact of positive resection margins on survival and recurrence following resection and adjuvant chemotherapy for pancreatic ductal adenocarcinoma. *Ann Surg.* 2019;269:520–529.
3. Zhang J-F, Hua R, Sun Y-W, et al. Influence of perineural invasion on survival and recurrence in patients with resected pancreatic cancer. *Asian Pac J Cancer Prev.* 2013;14:5133–5139.
4. Verbeke CS, Gladhaug IP. Resection margin involvement and tumour origin in pancreatic head cancer. *Br J Surg.* 2012;99:1036–1049.
5. Vahrmeijer AL, Hutteman M, van der Vorst JR, van de Velde CJH, Frangioni JV. Image-guided cancer surgery using near-infrared fluorescence. *Nat Rev Clin Oncol.* 2013;10:507–518.
6. Tipirneni KE, Warram JM, Moore LS, et al. Oncologic procedures amenable to fluorescence-guided surgery. *Ann Surg.* 2017;266:36–47.
7. Rosenthal EL, Warram JM, de Boer E, et al. Safety and tumor specificity of cetuximab-IRDye800 for surgical navigation in head and neck cancer. *Clin Cancer Res.* 2015;21:3658–3666.
8. Harlaar NJ, Koller M, de Jongh SJ, et al. Molecular fluorescence-guided surgery of peritoneal carcinomatosis of colorectal origin: a single-centre feasibility study. *Lancet Gastroenterol Hepatol.* 2016;1:283–290.
9. Koller M, Qiu S-Q, Linssen MD, et al. Implementation and benchmarking of a novel analytical framework to clinically evaluate tumor-specific fluorescent tracers. *Nat Commun.* 2018;9:3739.
10. van Dam GM, Themelis G, Crane LMA, et al. Intraoperative tumor-specific fluorescence imaging in ovarian cancer by folate receptor-α targeting: first in-human results. *Nat Med.* 2011;17:1315–1319.
11. Ellis LM, Hicklin DJ. VEGF-targeted therapy: mechanisms of anti-tumour activity. *Nat Rev Cancer.* 2008;8:579–591.
12. Tang R-F, Wang S-X, Peng L, et al. Expression of vascular endothelial growth factors A and C in human pancreatic cancer. *World J Gastroenterol.* 2006;12:280–286.

13. Nagakawa Y, Aoki T, Kasuya K, Tsuchida A, Koyanagi Y. Histologic features of venous invasion, expression of vascular endothelial growth factor and matrix metalloproteinase-2 and matrix metalloproteinase-9, and the relation with liver metastasis in pancreatic cancer. *Pancreas.* 2002;24:169–178.
14. Lamberts LE, Koch M, de Jong JS, et al. Tumor-specific uptake of fluorescent bevacizumab-IRDye800CW microdosing in patients with primary breast cancer: a phase I feasibility study. *Clin Cancer Res.* 2017;23:2730–2741.
15. Hartmans E, Tjalma JJJ, Linssen MD, et al. Potential red-flag identification of colorectal adenomas with wide-field fluorescence molecular endoscopy. *Theranostics.* 2018;8:1458–1467.
16. Ter Weele EJ, Terwisscha van Scheltinga AGT, Linssen MD, et al. Development, preclinical safety, formulation, and stability of clinical grade bevacizumab-800CW, a new near infrared fluorescent imaging agent for first in human use. *Eur J Pharm Biopharm.* 2016;104:226–234.
17. Adsay NV, Basturk O, Saka B, et al. Whipple made simple for surgical pathologists: orientation, dissection, and sampling of pancreaticoduodenectomy specimens for a more practical and accurate evaluation of pancreatic, distal common bile duct, and ampullary tumors. *Am J Surg Pathol.* 2014;38:480–493.
18. Hoogstins CES, Boogerd LSF, Sibinga Mulder BG, et al. Image-guided surgery in patients with pancreatic cancer: first results of a clinical trial using SGM-101, a novel carcinoembryonic antigen-targeting, near-infrared fluorescent agent. *Ann Surg Oncol.* 2018;25:3350–3357.
19. Tummers WS, Miller SE, Teraphongphom NT, et al. Intraoperative pancreatic cancer detection using tumor-specific multimodality molecular imaging. *Ann Surg Oncol.* 2018;25:1880–1888.
20. Koller M, Hartmans E, de Groot DJA, et al. Data-driven prioritization and review of targets for molecular-based theranostic approaches in pancreatic cancer. *J Nucl Med.* 2017;58:1899–1903.
21. de Geus SWL, Boogerd LSF, Swijnenburg R-J, et al. Selecting tumor-specific molecular targets in pancreatic adenocarcinoma: paving the way for image-guided pancreatic surgery. *Mol Imaging Biol.* 2016;18:807–819.
22. Hiroshima Y, Maawy A, Zhang Y, et al. Metastatic recurrence in a pancreatic cancer patient derived orthotopic xenograft (PDOX) nude mouse model is inhibited by neoadjuvant chemotherapy in combination with fluorescence-guided surgery with an anti-CA 19-9-conjugated fluorophore. *PLoS One.* 2014;9:1–13.
23. Hiroshima Y, Maawy A, Zhang Y, et al. Fluorescence-guided surgery in combination with UVC irradiation cures metastatic human pancreatic cancer in orthotopic mouse models. *PLoS One.* 2014;9:1–9.
24. Hiroshima Y, Maawy A, Zhang Y, et al. Fluorescence-guided surgery, but not bright-light surgery, prevents local recurrence in a pancreatic cancer patient derived orthotopic xenograft (PDOX) model resistant to neoadjuvant chemotherapy (NAC). *Pancreatology.* 2015;15:295–301.
25. Parsons CM, Sutcliffe JL, Bold RJ. Preoperative evaluation of pancreatic adenocarcinoma. *J Hepatobiliary Pancreat Surg.* 2008;15:429–435.
26. Handgraaf HJM, Boonstra MC, Prevoo HAJM, et al. Real-time near-infrared fluorescence imaging using cRGD-ZW800-1 for intraoperative visualization of multiple cancer types. *Oncotarget.* 2017;8:21054–21066.
27. Lu G, van den Berg NS, Martin BA, et al. Tumour-specific fluorescence-guided surgery for pancreatic cancer using panitumumab-IRDye800CW: a phase 1 single-centre, open-label, single-arm, dose-escalation study. *Lancet Gastroenterol Hepatol.* 2020;5:753–764.